AN IONIZED MICROJET FROM THE ORION NEBULA PROPLYD LV 2

W. J. Henney,[1] J. Meaburn,[2] and S. T. Garrington[2]

RESUMEN

Presentamos los resultados de observaciones a frecuencias múltiples del proplyd LV 2 (M42 167–317) en la nebulosa de Orión, concentrandonos sobre el analisís del "microjet" que sale del frente de ionización del proplyd. El jet es undireccional en su base pero se encuentran filamentos débiles y simétricos a ambos lados en escalas de arcosegundos. Estimamos las características físicas del jet a partir de las observaciones y lo comparamos con otros microjets irradiados.

ABSTRACT

We present results of multi-wavelength observations of the Orion nebula proplyd LV 2 (M42 167–317), concentrating on our analysis of the microjet that emerges from the proplyd's ionization front. The microjet is one-sided at its base but faint, symmetrical jet filaments are seen on both sides at arcsecond scales. The physical characteristics of the jet (opening angle, density, mass-loss rate, momentum-loss rate, luminosity) are estimated from the observations and compared with those of other irradiated microjets.

Key Words: **H II REGIONS — ISM: JETS AND OUTFLOWS — STARS: PRE-MAIN SEQUENCE — STARS: MASS LOSS**

1. INTRODUCTION

One of the brightest proplyds in the Orion Nebula is LV 2 (M42 167–317), which lies at a projected distance of $7\rlap{.}''8$ from θ^1 Ori C, the dominant ionizing star of the Trapezium cluster (corresponding to 5.05×10^{16} cm for an assumed distance of 430 pc). Like many of the Orion proplyds (e.g., Bally, O'Dell, & McCaughrean 2000; García-Arredondo, Henney, & Arthur 2001), LV 2 harbors a one-sided microjet, initially discovered via ground-based optical echelle spectroscopy (Meaburn 1988; Meaburn et al. 1993). In this contribution, we first (§ 2) summarize the results of a multi-wavelength observational campaign to study this fascinating object, presenting our results regarding the proplyd's jet in § 3. Further details plus discussion of our results on the proplyd's photoevaporation flow and standoff bowshock can be found in Henney et al. (2002, hereafter HOMGL). We then (§ 4) discuss the implications of our results for the nature of the microjet. This discussion is more extensive than that found in HOMGL.

2. OBSERVATIONAL DATA

2.1. *HST/STIS NUV Spectra*

We obtained *HST*/STIS near-ultraviolet MAMA E230H-mode echelle spectra in the density-sensitive doublet [C III] 1907 Å, C III] 1909 Å. The resolution of these observations is approximately 2.5 km s^{-1} ×

$0\rlap{.}''05$, adequately oversampled by the pixel size of 1.32 km s^{-1} × $0\rlap{.}''029$. The $0\rlap{.}''2 \times 6\rlap{.}''0$ slit was oriented along the axis of the proplyd, which coincides with the line to θ^1 Ori C. The full-resolution, rectified, and calibrated position-velocity images are shown in Figure 1a (note that the 1909 Å line was observed in two different orders and that the 1907 Å line is barely visible in the full-resolution data). The microjet is clearly visible at $\sim +130$ km s^{-1}. Figure 1b shows a zoomed-out view of the same data after boxcar smoothing by 22×15 pixels, allowing the 1907 Å line to be seen as well as fainter emission from the proplyd tail (offset $-1''$ to $0\rlap{.}''7$), standoff bowshock (offset $\sim 2\rlap{.}''5$) and background nebula (offset $< -1\rlap{.}''5$).

2.2. *HST/Planetary Camera Optical Images*

We have used publicly-available archival WFPC2 Planetary Camera images (program GO 5469, PI: John Bally) in the filters F502N ([O III] 5007 Å), F547M (visual continuum), F656N (Hα) and F658N ([N II] 6583 Å), which were flux-calibrated by Bob O'Dell using the method of O'Dell & Doi (1999). A three-color image of the proplyd and its environs is shown in Figure 2.

2.3. *MERLIN Radio Interferometry*

We carried out MERLIN 6 cm radio-interferometric observations of the Orion nebula for a total of 80 hours integration time. Further details of the data calibration and reduction are given in HOMGL. Figure 3a shows the resulting image of

---

[1]Instituto de Astronomía, UNAM, Morelia, México.
[2]Jodrell Bank Observatory, U. Manchester, UK.
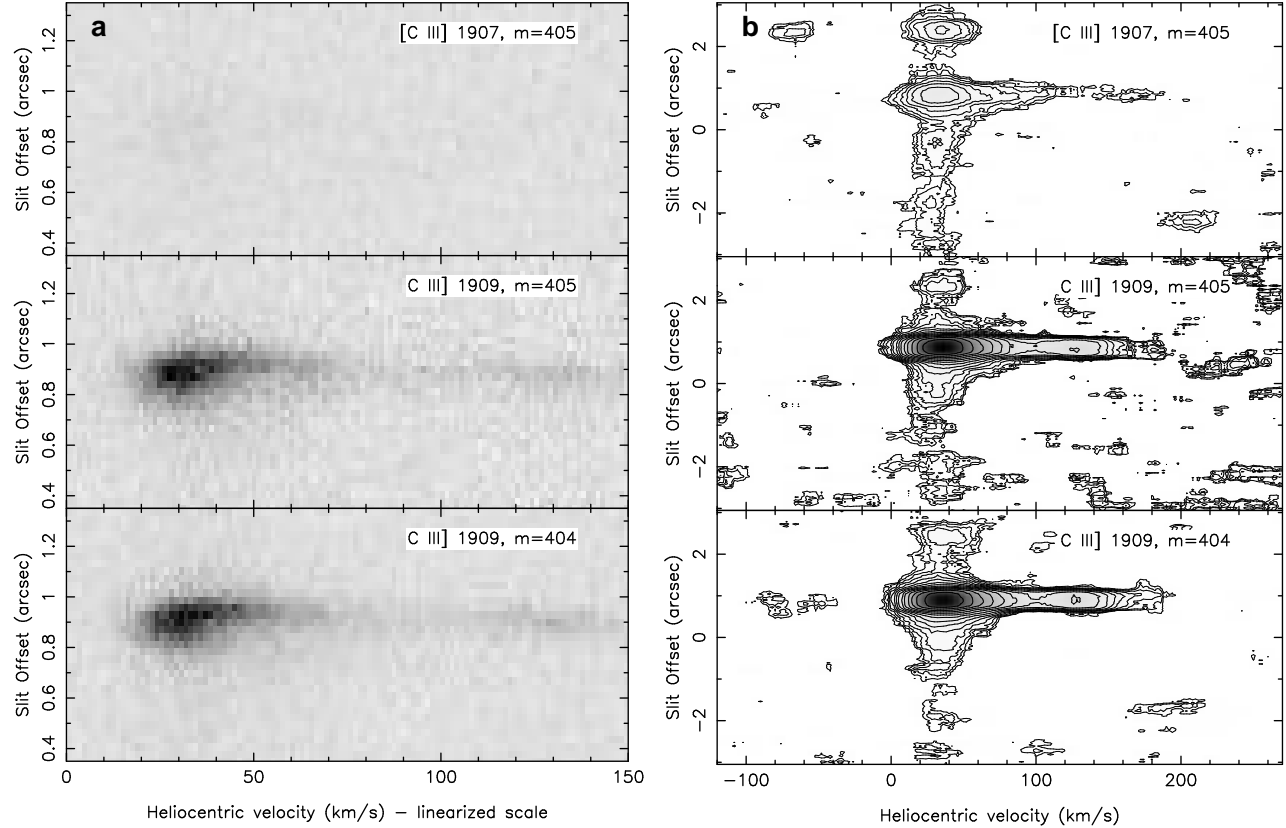
Fig. 1. (a) Raw position-velocity images showing the NUV C III lines observed with STIS. (b) Boxcar-smoothed ($30 \text{ km s}^{-1} \times 0''\!.435$) position-velocity images of the same data as in (a), but for a wider range in position and velocity.

LV 2, deconvolved with a circular restoring beam of FWHM 80 mas. The peak radio surface brightness is 1.3 mJy/beam, while the RMS noise is 0.05 mJy/beam and the alignment between optical and radio images is expected to be good to 20 mas.

2.4. *Groundbased Optical Spectra*

We obtained longslit [O III] 5007 Å observations of LV 2 with Manchester Echelle spectrograph on the 2.1 m telescope of the Observatorio Astronómico Nacional, San Pedro Mártir, B.C., México. The resulting extracted proplyd line profile (velocity resolution $\simeq 6 \text{ km s}^{-1}$) is shown in Fig. 2 of HOMGL.

3. ISOLATION OF THE JET EMISSION

Isolation of the jet emission from that of the low-velocity proplyd photoevaporation flow in the spectral data is relatively straightforward due to the very different kinematics of the two flows. This is illustrated in Figure 4, where the solid line shows the predicted line profile from a proplyd model that has been fitted to the *HST* emission line images. This model can explain all the C III emission blueward of $+40 \text{ km s}^{-1}$. The emission redward of $+75 \text{ km s}^{-1}$ can be safely ascribed to the jet, although the nature of the emission intermediate between these two velocities is uncertain. It is possible that this emission comes from a lower-velocity, less-collimated jet component, as is often seen in small-scale outflows from T Tauri stars (see, e.g., Ray & Mundt, this volume). On the other hand, the proplyd model does not include the effects of scattering by dust grains (e.g., Henney 1998), which might be expected to give a broad red shoulder to the profile from the photoevaporation flow, possibly explaining the excess emission around $+50 \text{ km s}^{-1}$. More interesting possibilities, such as the entrainment of part of the proplyd flow by the jet, also cannot be ruled out. There is no conclusive evidence from either the STIS (HOMGL) or ground-based spectra (Meaburn et al. 1993) of any blue-shifted emission from the jet (see discussion in HOMGL).

A stubby spike can be seen to protrude from the SE side of the proplyd ionization front in the log-scale inset images of Figure 2 (labelled "Jet base" in the right-hand image). No such spike is visible on the
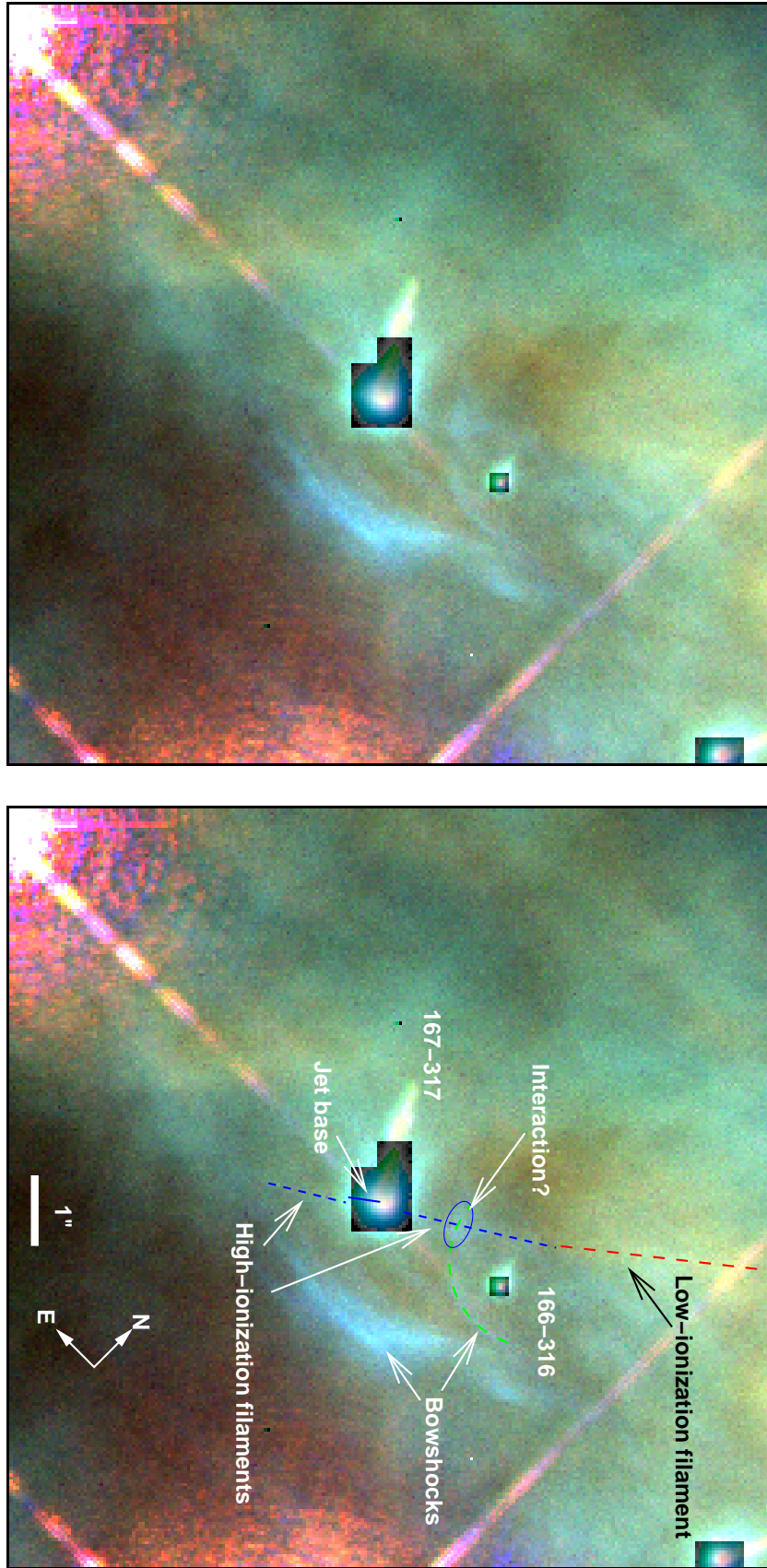
Fig. 2. Three-color *HST*/PC image of LV 2 and its immediate surroundings. Red is [N II] 6583 Å, green is Hα, and blue is [O III] 5007 Å. The main image is on a linear scale, tuned to emphasize the fainter features, whereas inset boxes are on a logarithmic scale, showing the far brighter emission from the proplyd ionization fronts. The right panel shows various features of interest (see text for discussion). The pink-colored bright linear features at ±45° angles are stellar diffraction spikes. NOTE: THIS FIGURE IS AVAILABLE IN COLOR IN THE ELECTRONIC VERSION OF THIS ARTICLE, OBTAINABLE FROM http://www.astroscu.unam.mx/~rmaa/.
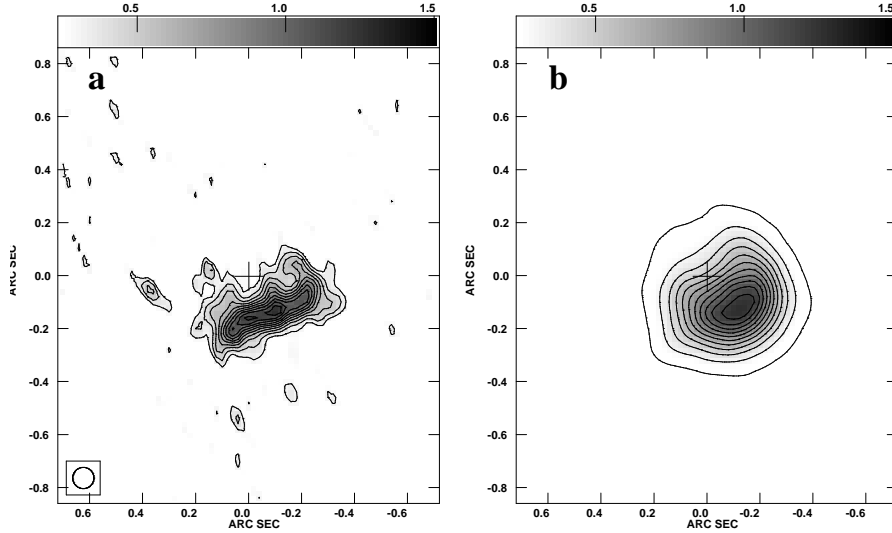
Fig. 3. (a) MERLIN image of LV 2 at a resolution of 80 mas. The contour levels are at intervals of 0.1, beginning at 0.3 mJy/beam. (b) The 6 cm image predicted from *HST* Hα images after normalizing to the same peak as the MERLIN image. The contour levels are in steps of 0.1.

NW side. Also, faint filaments can be clearly seen in Figure 2, extending approximately 1″5 on each side of the proplyd, with the filament brightnesses on the two sides being approximately equal.

The blue color of the jet filaments indicates that the emission is predominantly [O III] and Hα, with almost no [N II] emission. The emission-line ratios are consistent with those expected from optically thin photoionized gas at the observed distance from θ^1 Ori C. There is no evidence that shock excitation contributes significantly to the observed emission.

Interestingly, on the NW side of the proplyd, the jet filament seems to brighten at the position where it intersects the standoff bowshock of another proplyd, 166–316, possibly indicating an interaction with the bowshock shell. Also, just beyond 166–316, and with the same general orientation as the high-ionization jet filament, lies a lower-ionization filament (with a greenish-yellow color in the image). It is not clear, however, whether this filament is physically related to the proplyd jet. Similar features are quite common in the Orion nebula: some are probably due to "escarpments" or ridges in the principal ionization front of the nebula (O'Dell & Yusef-Zadeh 2000); others may be the ionization shadows of proplyds or other optically-thick objects embedded in the nebula (O'Dell 2000). If the low-ionization filament *is* due to the jet, then it would imply that the jet were directed away from the observer on the NW side. The transition from high- to low-ionization could then be understood as the point where the jet passes from the He$^+$ zone of the nebula interior into the He^0 zone near the background ionization front. However, this would then be inconsistent with the fact that the

emission from the jet base is both exclusively redshifted and exclusively to the SE.

To further isolate the emission from the base of the jet, we have exploited the fact that the underlying low-velocity photoevaporation flow emission has approximate mirror-symmetry about the proplyd axis (which is aligned with the direction to the exciting star, θ^1 Ori C). Since the base of the jet is one-sided, it should show up clearly as an asymmetry in the emission-line images. Figure 5 shows the fractional asymmetry of the Hα, [O III] and [N II] lines. The fractional asymmetry is defined as $(S - \widetilde{S})/\widetilde{S}$ where S is the surface brightness of the original image and $\widetilde{S}$ is the surface brightness of an image that has been reflected about the proplyd axis (dashed line). The most prominent asymmetric features in the head of the proplyd is indeed seen to be the jet, although the "wiggle" in the tail also shows up. The Hα image has probably the best signal-to-noise and shows a narrow spike of high fractional asymmetry ($\simeq 1$–1.5), which extends from $r \simeq 2r_0$ (where r_0 is the ionization front radius) out to as far as can be reliably measured, implying a jet projected half opening angle of no more than $\sim 10°$. A broader cone of lower fractional asymmetry ($\simeq 0.5$) is also seen, particularly at larger radii ($\simeq 4r_0$), but the emission here is faint and it may not be connected with the jet. Almost exactly the same pattern of asymmetry is seen in the other two lines, although somewhat less clearly. It is interesting that in all 3 cases the fractional asymmetry is weak close to the ionization front, becoming stronger at larger radii. A possible explanation for this is presented in § 4 below.
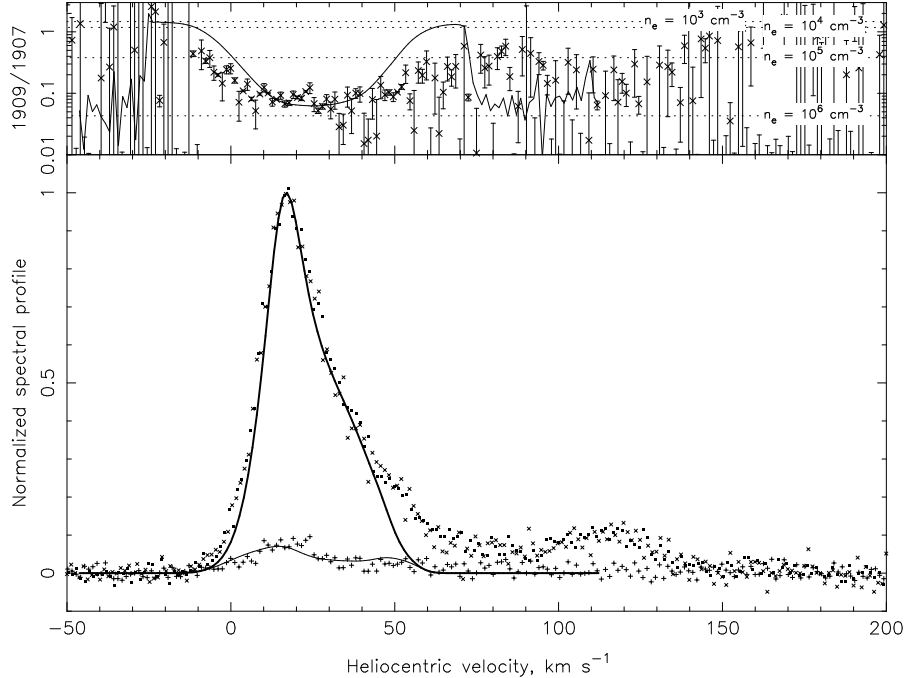
Fig. 4. Comparison of observed C III] 1909 Å and [C III] 1907 Å profiles of the proplyd head (symbols) with predictions of a photoevaporation model (line). The upper panel shows the density-sensitive ratio of the two lines. Smoothed versions of these line profiles are shown in Fig. 4 of HOMGL.

Significant differences are apparent between the 6 cm radio map of the proplyd/jet and the 6 cm map that would be predicted from the Hα image, assuming isothermal free-free emission (see Fig. 3). In particular, the jet is relatively brighter at 6 cm, compared to the emission from the photoevaporation flow. This may be indicative of non-thermal radio emission from the jet (see discussion in HOMGL) but observations of comparable resolution at other radio frequencies are required to confirm this. Similar puzzling discrepancies between the Hα and radio emission have also been found for the interproplyd shell in the interacting proplyd binary system LV 1 (Graham et al. 2002; Henney 2002).

4. DERIVED PHYSICAL PARAMETERS FOR THE LV 2 JET

In this section, we make estimates of the physical properties of the ionized jet from LV 2, based on our observations. In particular, we derive values for the jet's mass-loss rate, $\dot{M}_{\rm j}$, momentum-loss rate, $\dot{P}_{\rm j}$, and mechanical luminosity, $L_{\rm j}$. In order to simplify the analysis, we make the following working assumptions. We assume that the jet is straight and inclined at an angle, $i_{\rm j}$, with respect to the line of sight, with constant velocity ($v_{\rm j}$) and temperature equal to the photoionization equilibrium value of $\simeq 10^4$ K. We further assume that the ionization front in the jet occurs at the same radius as that in the proplyd flow, r_0, and that the jet has a constant opening half-angle, $\theta_{\rm j}$, equal to the Mach angle: $\sin \theta_{\rm j} = c_0/v_{\rm j}$, with the jet density being homogeneous across its

cross section at each radius. Observational tests of these assumptions are examined below.

The fundamental observational quantities used in this analysis are as follows:

1. The electron density in the jet $n_{\rm j,0}$ at the point where it crosses the ionization front, determined to be $\simeq 10^6$ cm^{-3} from the C III]/[C III] intensity ratio (see Figure 4 of HOMGL).

2. The radius of the ionization front, $r_0 \simeq 8 \times 10^{14}$ cm, found from model fits to the *HST* images.

3. The projected radial velocity of the jet with respect to the proplyd's systemic velocity, $v_{\rm j,rad} \simeq 100$ km s^{-1}, determined from the [O III] 5007 Å and C III] 1909 Å line profiles (§§ 2.1, 2.4). This is related to the true jet velocity by $v_{\rm j,rad} = -v_{\rm j} \cos i_{\rm j}$.

4. The total flux, $F_{\rm j}$, of the jet emission in the [O III] 5007 Å and C III] 1909 Å lines, relative to the flux, $F_{\rm p}$, of the same line from the proplyd photoevaporation flow. This is $F_{\rm j}/F_{\rm p} \simeq 0.05$ for [O III] 5007 Å and $F_{\rm j}/F_{\rm p} \simeq 0.1$ for C III] 1909 Å (Fig. 4).

5. The jet surface brightness, $S_{\rm j}$, as a function of projected radius in the Hα, [O III] 5007 Å, and [N II] 6583 Å lines, relative to the surface brightness, $S_{\rm p}$, of the proplyd photoevaporation flow (Figure 5).

6. An upper limit to the projected opening half-angle, $\theta'_{\rm j}$, also determined from the *HST* images. This is related to the true opening half-angle by $\sin \theta'_{\rm j} = \sin \theta_{\rm j} / \sin i_{\rm j}$.

The mass-loss rate in the jet is given by $\dot{M}_{\rm j} = \mu m_{\rm H} n_{\rm j,0} r_0^2 v_{\rm j} \Omega_{\rm j}$, where $\Omega_{\rm j} = 2\pi(1 - \cos \theta_{\rm j}) \simeq \pi \theta_{\rm j}^2$, while the momentum-loss rate and mechanical lumi-
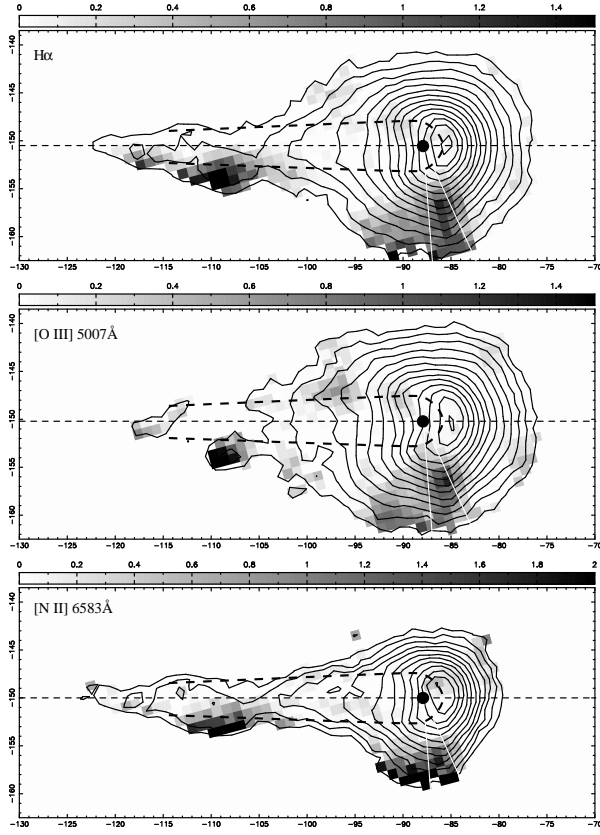
Fig. 5. Linear grayscale image of the fractional asymmetry of the proplyd in each emission line, shown superimposed on contours of surface brightness. The approximate opening cone of the jet is shown by white lines, suggesting a projected half opening angle $< 10°$, although there is also the hint of a fainter, wider-angle flow. The approximate position of the ionization front is shown by heavy dashed lines.

nosity are given by $\dot{P}_j = \dot{M}_j v_j$ and $L_j = 0.5\dot{M}_j v_j^2$. Substituting the observational data 1–3 above then gives $\dot{M}_j \simeq 10^{-8}|\cos i_j|M_\odot$ yr^{-1}, $\dot{P}_j \simeq 6 \times 10^{24}$ dyne, $L_j \simeq 0.8|\cos i_j|^{-1}L_\odot$. Note that there is a residual uncertainty in these numbers (except for the momentum rate) due the unknown jet inclination angle. Furthermore, they are obviously only as good as the assumptions used in their derivation. It is therefore worthwhile to attempt to constrain i_j and test these assumptions by using the remaining observational data 4–6 given above.

We will explore 3 different possibilities for the jet inclination, denoted Case A, B, and C, with $\cos i_j = [-0.25, -0.5, -0.75]$, respectively. Given that the jet is observed to be receding ($\cos i_j < 0$) these 3 cases uniformly cover the a priori distribution of expected jet orientations in the absence of strong selection effects. The true jet velocity is then $v_j =$

[400, 200, 133] km s^{-1} and the true and observed opening angles (assuming the simple Mach cone discussed above) are $\theta_j = [1.7°, 3.4°, 5.2°]$, $\theta'_j = [1.7°, 4.0°, 7.8°]$. All three values for θ'_j are consistent with the upper limit determined from the *HST* images of $\theta'_j < 10°$.

Ignoring collisional deexcitation and dust extinction, the total flux from the jet in a given emission line will be $F_j \propto \Omega_j n_{j,0}^2 r_0^3$, whereas the equivalent flux from the head of the proplyd will be $F_p \propto \pi \xi_p n_{p,0}^2 r_0^3$ with the same constant of proportionality, where $\xi_p \simeq 0.17$ is a dimensionless parameter that accounts for the steeper-than-r^{-2} decline in the density of the photoevaporation flow. Hence, the jet opening angle can be estimated as $\theta_j \simeq 24(F_j/F_p)^{1/2}(n_{j,0}/n_{p,0})^{-1}$ degrees. Using the values for the [O III] 5007 Å and C III] 1909 Å lines given above, together with the value $n_{j,0}/n_{p,0} \simeq 1$ then gives $\theta_j \simeq 5°$–$8°$. The ground-based [O III] 5007 Å value is probably the more reliable since in this case all of the proplyd and jet fall within the slit, which would give the lower end of the range for θ_j. This is most consistent with Case C for the jet orientation, which has the jet at a relatively large angle to the plane of the sky. Any refinements in the estimate of F_j/F_p are only likely to strengthen this conclusion: dust extinction, if important, will effect the (receding) jet more than it effects the (largely approaching) proplyd flow, leading to a true F_j/F_p that is larger than that observed.

Similarly, the surface brightness of the jet in a given emission line can be written as $S_j \propto 2\tan\theta_j r_0 n_{j,0}^2 \sin^2 i_j x^{-3}$, where x is the projected radius in units of r_0, whereas the surface brightness of the proplyd flow in the same line will be $S_p \propto \zeta_p r_0 n_{p,0}^2 M_p^{-2} x^{-3}$, where M_p is the Mach number of the photoevaporation flow at radius xr_0 and $\zeta_p \simeq 0.5$ is a dimensionless factor representing the line-of-sight integral through the photoevaporation flow at the projected position angle of the jet. Hence, a further estimate of the jet opening angle can be obtained: $\theta_j \simeq 14.5(S_j/S_p)(n_{j,0}/n_{p,0})^{-2}M_p^{-2}\sin^{-2} i_j$ degrees. Fig. 5 shows that $S_j/S_p \simeq 1$ in all 3 emission lines at a projected radius of 2–3r_0, at which point $M_p \simeq 2.5$ is expected, which implies $\theta_j \simeq [2.5°, 3.1°, 5.3°]$ for Cases A, B, and C. This is compatible with the predicted opening angles for all three cases, so cannot be used to discriminate between them. On the other hand, It is gratifying that three quite separate methods for determining θ_j all give compatible answers, implying that the working assumptions given at the start of this section are not too wide of the mark. Further-

more, the images of S_j/S_p (Fig. 5) allow more specific tests of these assumptions. The transsonic proplyd flow accelerates sharply from $M_p = 1$ at r_0 up to $M_p = 2$ by $1.5r_0$, followed by a slower acceleration up to $M_p = 3$ by $4r_0$. Hence, given our supposition that the jet density is $\propto r^{-2}$, S_j/S_p is expected to increase by roughly an order of magnitude between one and a few times r_0 and be roughly constant thereafter. Just such a behavior is seen in the images, lending support to our assumption of constant jet velocity and opening angle. It is also obvious from the figures that neither the pattern nor the absolute value of S_j/S_p shows any significant variation between the different emission lines. This argues in favor of our assumption that the jet temperature is roughly constant and the same as that of the proplyd flow. In particular, if the jet temperature were significantly higher than 10,000 K, then one would expect a far smaller asymmetry in the Hα recombination line image than in the collisionally excited lines, [N II] and [O III].

A further argument in favor of a low value for $\sin i_j$ (as in Case C above) is the fact that the jet is observed with STIS *at all*. This is because the STIS slit has a width of only $\Delta = 0.2''$ whereas the ionization front radius is $r_0 \simeq 0.125''$ and the jet PA is at an angle of $\phi \simeq 80°$ to the slit axis. The fraction of the jet flux that enters the STIS slit is approximately $1–2r_0 \sin\phi \sin i_j/\Delta$. This is zero for $\sin i_j > 0.81$, which would rule out Cases A and B, and is only 20% for Case C, indicating that $\sin i_j$ may be even lower than in this case.

5. DISCUSSION

The jet mass-loss rate found from our analysis is within a factor of two of the value obtained by Bally et al. (2000), who used a more approximate method, and similar values are found for other irradiated jets in the Orion nebula and other H II regions. These irradiated jets are much less powerful than those that drive "classical" Herbig-Haro outflows, which may be due to the greater ages (Bally et al. 2000) or smaller masses (HOMGL) of their central stars.

Possible reasons for the one-sided nature of an irradiated jet are discussed in Bally & Reipurth (2000, 2002) and in HOMGL. A possibly unique feature of the the LV 2 jet is that the jet asymmetry seems to be confined to its base: the arcsecond-scale fil-

aments are roughly symmetrical (see Figure 2). This suggests that the emission mechanisms working in the two parts of the jet are different: mainly photoionization at the base but largely shock excitation in the larger-scale filaments (although it should be noted that there is as yet no direct evidence for shock excitation of the filaments). Then, as pointed out in HOMGL, the symmetrical outer filaments would imply that the jet mechanical luminosity be equal on the two sides. In turn, this would mean that the (photoionized) base of the jet should be brighter on the side that has the *lower* jet velocity. Interestingly, this case is different from any of the 3 cases discussed by Bally & Reipurth. Deep, high-resolution, spectroscopic observations are required in order to try and detect the blue-shifted counterjet emission and test this hypothesis.

REFERENCES

Bally, J., O'Dell, C. R., & McCaughrean, M. J. 2000, AJ, 119, 2919
Bally, J., & Reipurth, B. 2000, ApJ, 546, 299
———. 2002, RevMexAA(SC), 13, 1 (this volume)
García-Arredondo, F., Henney, W. J., & Arthur, S. J. 2001, ApJ, 561, 830
Graham, M. F., Meaburn, J., Garrington, S. T., O'Brien, T. J., Henney, W. J., & O'Dell, C. R. 2002, ApJ, 570, 222
Henney, W. J. 1998, ApJ, 503, 760
Henney, W. J., O'Dell, C. R., Meaburn, J., Garrington, S. T., & López, J. A. 2002, ApJ, 566, 315 (HOMGL)
Henney, W. J. 2002, RevMexAA, 38, 71
Meaburn, J. 1988, MNRAS, 233, 791
Meaburn, J., Massey, R. M., Raga, A. C., & Clayton, C. A. 1993, MNRAS, 260, 625
O'Dell, C. R. 2000, AJ, 119, 2311
O'Dell, C. R. & Doi, T. 1999, PASP, 111, 1316
O'Dell, C. R. & Yusef-Zadeh, F. 2000, AJ, 120, 382
Ray, T., & Mundt, R. 2002, RevMexAA(SC), 13, 83 (this volume)

W. J. Henney: Instituto de Astronomía, Universidad Nacional Autónoma de México, Campus Morelia, Apartado Postal 3–72, 58090 Morelia, Michoacán, México (w.henney@astrosmo.unam.mx).
J. Meaburn and S. T. Garrington: Jodrell Bank Observatory, University of Manchester, Macclesfield, Cheshire SK11 9DL, UK (jm,stg@ast.man.ac.uk).